Contrast agent-free sonoporation: The use of an ultrasonic standing wave microfluidic system for the delivery of pharmaceutical agents

Dario Carugo,[1,b)] Dyan N. Ankrett,[2,a),b)] Peter Glynne-Jones,[2] Lorenzo Capretto,[1] Rosemary J. Boltryk,[2] Xunli Zhang,[1] Paul A. Townsend,[3] and Martyn Hill[2]
[1]*Bioengineering Group, Engineering Sciences, University of Southampton, Southampton SO17 1BJ, United Kingdom*
[2]*Electromechanical Engineering Group, Engineering Sciences, University of Southampton, Southampton SO17 1BJ, United Kingdom*
[3]*Cancer Sciences, Faculty of Medicine, University of Southampton, Southampton SO16 6YD, United Kingdom*

(Received 24 August 2011; accepted 25 October 2011; published online 15 November 2011)

Sonoporation is a useful biophysical mechanism for facilitating the transmembrane delivery of therapeutic agents from the extracellular to the intracellular milieu. Conventionally, sonoporation is carried out in the presence of ultrasound contrast agents, which are known to greatly enhance transient poration of biological cell membranes. However, *in vivo* contrast agents have been observed to induce capillary rupture and haemorrhage due to endothelial cell damage and to greatly increase the potential for cell lysis *in vitro*. Here, we demonstrate sonoporation of cardiac myoblasts in the absence of contrast agent (CA-free sonoporation) using a low-cost ultrasound-microfluidic device. Within this device an ultrasonic standing wave was generated, allowing control over the position of the cells and the strength of the acoustic radiation forces. Real-time single-cell analysis and retrospective post-sonication analysis of insonated cardiac myoblasts showed that CA-free sonoporation induced transmembrane transfer of fluorescent probes (CMFDA and FITC-dextran) and that different mechanisms potentially contribute to membrane poration in the presence of an ultrasonic wave. Additionally, to the best of our knowledge, we have shown for the first time that sonoporation induces increased cell cytotoxicity as a consequence of CA-free ultrasound-facilitated uptake of pharmaceutical agents (doxorubicin, luteolin, and apigenin). The US-microfluidic device designed here provides an *in vitro* alternative to expensive and controversial *in vivo* models used for early stage drug discovery, and drug delivery programs and toxicity measurements. [doi:10.1063/1.3660352]

I. INTRODUCTION

Gas-filled ultrasound contrast-agent microbubbles (UCA or CA) have been used for many decades in diagnostic imaging as they are effective back-scatterers of ultrasound (US) in perfused tissue.[1] More recently, CAs are being explored experimentally, both *in vitro*[2] and *in vivo*,[3] and pre-clinically for their therapeutic potential in the expanding fields of targeted gene, antibody, and drug delivery.[4,5] In particular, at specific ultrasonic frequencies, resonant CAs are known to drastically enhance transient poration of biological cell membranes (sonoporation).[6]

[a)]Author to whom correspondence should be addressed. Electronic mail: D.Ankrett@soton.ac.uk. Telephone: +44 (0) 2380592427.
[b)]Dario Carugo and Dyan N. Ankrett contributed equally to this work.

Sonoporation is a useful biophysical mechanism for facilitating the transmembrane delivery of therapeutic agents from the extracellular to the intracellular milieu. Other techniques for facilitating the transmembrane delivery of bioactive molecules include electroporation using high intensity electric fields to reversibly permeabilize cell membranes,[7] microinjection using micromanipulators and microneedles to inject molecules directly into the cell[8] and laser irradiation using a focused laser beam to induce membrane permeabilization.[9] However, sonoporation uses ultrasound to create transient membrane pores and is referred to as a "gentle" technique for facilitating transmembrane delivery.[10]

One of the accepted hypotheses is that sonoporation occurs by non-thermal acoustic cavitation, whereby air or gas bubbles under acoustic wave excitation form cavitation nuclei.[11] Intrinsic formation of "free" gas bubbles within living tissue is rare, with the exception of lung and intestinal tissue.[12] Additionally, free gas bubbles are unstable in liquid and will rapidly dissolve as a consequence of surface tension at the gas-liquid interface. As such, stabilised CAs (gas bubbles encapsulated with albumin, galactose, lipid, or polymer shells) are intentionally introduced into tissue to enhance ultrasound back-scatter, yielding high quality imaging.[13] Such CAs are micrometer size (1-10 μm diameter) allowing safe medical applications. The dynamic behaviour of CAs in an ultrasound field is size-, shell-, and gas composition-dependent. Capturing the dynamics of CAs experimentally usually requires high-speed photographic imaging techniques.[14] However, generally at low acoustic pressures CAs oscillate stably (non-inertial cavitation) but as the driving pressure increases more complex non-linear interactions occur. At relatively high pressure amplitudes CAs expand in volume, followed by rapid contraction and "violent" collapse (inertial cavitation). CA collapse has been observed to induce capillary rupture and haemorrhage due to endothelial cell damage *in vivo* and to greatly increase the potential for cell lysis *in vitro*.[15] However, CA collapse (also called ultrasound targeted microbubble destruction or UTMD) is also exploited for local drug and gene delivery. The underlying mechanisms involved in delivery are cavitation and formation of microjets creating micropores in cell membranes by high amplitude oscillations induced by ultrasonic frequencies that are traditionally used in myocardial contrast echocardiography (MCE).[16] UTMD can be applied to any US accessible or well-perfused tissue; however, cardiac applications are leading this field of research due to its origin in MCE and accessibility of the heart.[17]

Cardiovascular drug delivery programs and toxicity measurements generally involve the sacrifice of many animals. Additionally, cardiac cell isolation is a complex, multi-step process.[18] Therefore H9c2, a commercially available myogenic cell line derived from embryonic rat heart ventricle,[19] and which has reportedly comparable levels of drug metabolising enzymes,[20] provides a valuable *in vitro* alternative to the use of rat hearts and thus reducing reliance on *in vivo* research. This may contribute, at least in some way, to the 3Rs philosophy (reduction, refinement, and replacement of animal experiments),[21] which is also in line with a national centred UK government-sponsored scientific organisation, NC3Rs.[22]

Our experimental work aims to demonstrate the intracellular delivery of pharmaceutical agents to cardiac myoblasts by non-inertial CA-free sonoporation. An ultrasonic standing wave (USW) was generated within a biocompatible microfluidic device, which enables high cell viability to be maintained.

The first notable study utilising USW to induce sonoporation was by Khanna *et al.*[23] where CA was used to induce haemoglobin release from blood cells. Whilst this effect was largely attributed to cavitation, there were also indications that the cells were being stressed whilst travelling towards the nodal plane, but only in the presence of CA. Interestingly, Lee and Peng[24] and Rodamporn *et al.*[25] have both reported successful cellular gene transfection by sonoporation within a USW but in the absence of CA. Lee and Peng attribute their success to streaming around cells trapped at the nodal plane; however, no direct evidence of streaming was presented. More recently, Kinoshita and Hynynen[26] and Hassan *et al.*[27] have concluded that USWs increase sonoporation but typically at the expense of viability. However, Rodamporn's detailed study of operating conditions does suggest that careful selection of conditions can limit loss of viability whilst retaining high transfection rates.[25]

Following Rodamporn's study, we carefully considered the microfluidic device design in order to provide a low-stress, biocompatible environment for the cells within the ultrasonic field.[28] Microfluidic-based systems offer advantages over conventional bench systems in terms of performance, reduced sample/solvent quantity, automation, and fine regulation of the boundary conditions.[29,30] The micro-scale, in which fluidics is restricted to laminar flow and diffusive mixing, allows precise control of the physical parameters within the fluidic environment. In addition, coupling with microscope-based imaging techniques, provides a platform for *in situ* analysis of individual cells exposed to US or other physico-chemical stimuli.[31,32]

Within our device, an USW was generated to induce sonoporation and also to control the position of the cells. Acoustic radiation forces experienced by the cells move them reliably to an acoustic pressure node, mid-plane of the fluid chamber, in a single focal plane suitable for microscope observation. Additionally, our device is an easy-to-use and cost-effective miniaturised system for facilitating drug uptake, and which potentially offers an alternative to more expensive macro scale systems or animal models, which are routinely used in early stage drug screening and drug delivery programs. The device also has scope for coupling with other high resolution technologies and may assist high throughput screening.

To the best of our knowledge, we are the first research team to demonstrate facilitated drug up-take, resulting from CA-free sonoporation, by cytotoxic measurements pre- and post-sonications.

II. MATERIALS AND METHODS

CA-free sonoporation [Fig. 1(a)] was investigated by either real-time *single-cell* analysis or *retrospective* post-sonication analysis, using low-, intermediate-, and high- molecular weight therapeutic agents or fluorescent probes employed as a traceable model of bioactive molecules. A microfluidic approach, based on a cost-effective and easy-to-use experimental platform, was adopted to assess CA-free sonoporation of suspended cells.

A. General reagents

Dimethylsulfoxide(DMSO), trypsin-EDTA, trypan-blue (0.4%), MTT (3-[4,5-dimethylthiazol-2-yl]-2,5-diphenyltetrazolium bromide, a yellow tetrazolium salt, reduced by mitochondrial dehydrogenase of viable cells, forming an insoluble intracellular purple formazan product), FITC-dextran (dextran labelled with fluorescein isothiocyanate), doxorubicin, apigenin, luteolin, glycerol, foetal calf serum (FCS), Dulbecco's Modified Eagle's Medium for cell culture (DMEM) and penicillin-streptomycin were purchased from Sigma-Aldrich (Dorset, UK). 5-chloromethylfluorescein diacetate (CMFDA, Cell Tracker Green) and propidium iodide (PI) were purchased from Invitrogen (Paisley, UK). Optison™ gaseous CA (3.0-4.5 μm diameter) was purchased from GE Healthcare (Hatfield, UK). H9c2 cardiac myoblast cells were obtained from Southampton General Hospital (Southampton, UK).

B. Ultrasonic microfluidic device for CA-free cell sonoporation

The ultrasonic microfluidic device used in this study consisted of a disposable glass microcapillary (length: 30 mm, width: 6 mm, inside height: 300 μm, and glass thickness: 300 μm—VitroCom, Ilkley, UK) acoustically coupled to a piezoelectric transducer (PZT; PZ26 Ferroperm, Kvistgard, Denmark) by means of a thin film of glycerol. The transducer (length: 20 mm, width: 6 mm, and height: 1 mm) was held in place by a poly-methyl methacrylate (PMMA) spring loaded clamp [Fig. 1(b)] and driven by an RF power amplifier (240 L ENI, Rome, Italy) fed from a signal generator (TG103 TTI, Cambridgeshire, UK). An USW was generated within the microfluidic device at a resonant frequency determined through electrical impedance measurements (C-60, impedance analyser, Cypher Instruments Ltd., London, UK). This configuration allowed cells to migrate towards a nodal plane equidistant from the top and bottom surfaces of the capillary [Fig. 1(c)].[33] All cells flowing through the acoustic environment experience similar USW levels, as the device design allows spatial averaging. The acoustic pressure (P) within the

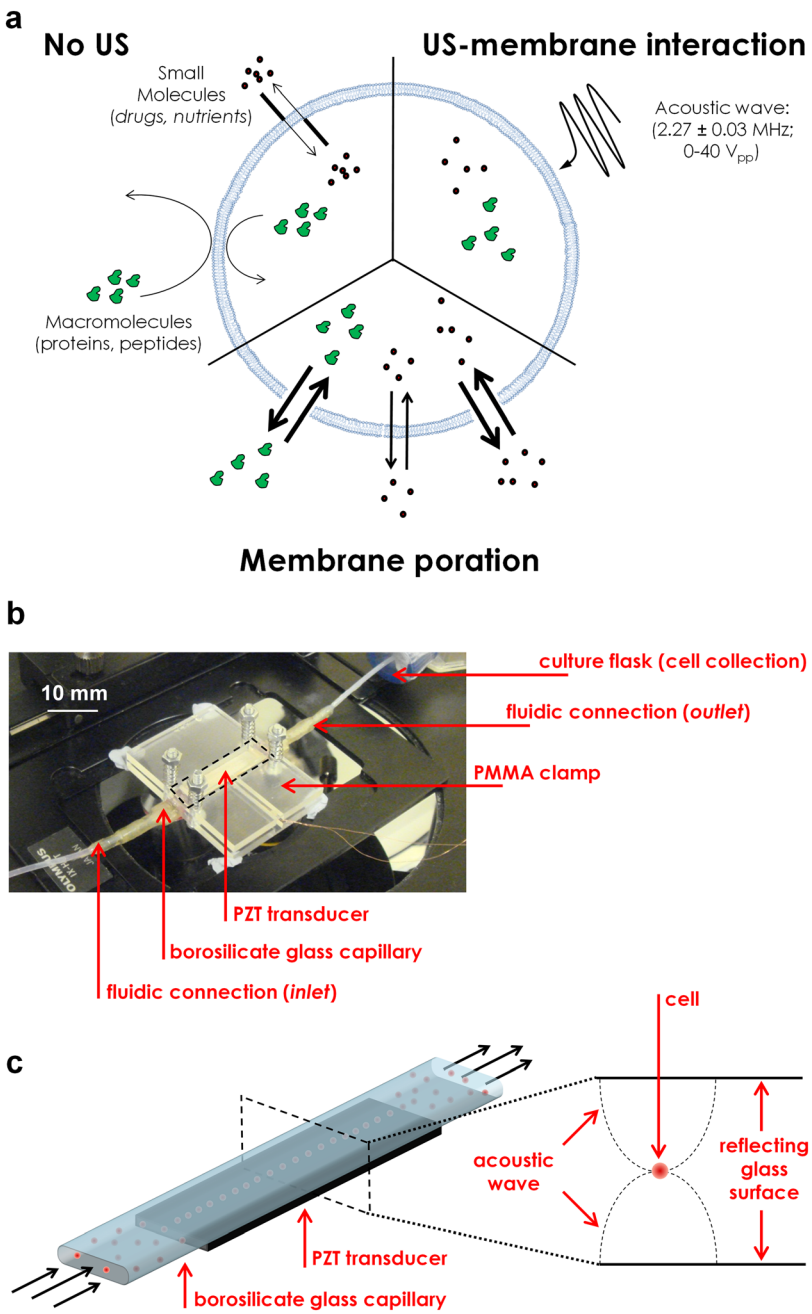

FIG. 1. (a) Schematic representation of the phenomena under investigation. Under normal condition (no US), the cell membrane is either impermeable or selectively permeable to small- and macro-molecules (i.e., bio-active or probe molecules) (top-left). An USW was applied to cells suspended within the microfluidic environment in the absence of CA. The ultrasonic wave interacts with cell membrane (US-membrane interaction) through mechanisms that remain widely uninvestigated. Both thermal and non-thermal mechanisms may contribute to membrane permeabilization (top-right). US exposure allows the transmembrane transfer of molecules, occurring through the formation of membrane pores (membrane poration) (bottom). (b) Microdevice photograph. Cells were injected within the microfluidic device through silicon fluidic connections and collected in a sterile culture flask. The device was placed on the stage of an inverted microscope. (c) When actuation matched the resonance condition in the capillary (resonance frequency, $f_R = 2.27$ MHz), a localized standing wave was generated above the transducer. Acoustic radiation forces experienced by the cells move them reliably to an acoustic pressure node in a single focal plane suitable for microscope observation.

capillary was measured through a drop-voltage analysis, using 20 μm diameter fluorescent polystyrene beads.[34] Polyofelin heat shrink tubing was used to stabilize silicon inlet and outlet tubing (1.6 mm OD, 1 mm ID) for fluid delivery and release [Fig. 1(b)]. All tubing was used with a minimum length in order to minimize cell sedimentation. A continuous-flow ($Q_{in} = 0.1$ ml/min; Reynolds number, $\mathrm{Re} = 0.53$) was established within the microdevice by means of a syringe pump (KD100, KD Scientific Inc., Holliston) allowing the processing of the relatively large numbers of cells (0.2×10^6 cells/min) required for the present study. The continuous-flow configuration is particularly advantageous for processing large numbers of cells compared with microinjection and laser configured systems, in which only single cells or low cell numbers can be processed.[35]

C. Preparation of cells for ultrasound assays

H9c2 cardiomyoblasts were selected as a biological model to investigate CA-free sonoporation of suspended cells within our microdevice. H9c2 cells were routinely cultured in DMEM culture medium supplemented with 10% (v/v) foetal calf serum and 1% (v/v) penicillin-streptomycin. Cells were maintained at 37 °C, 5% CO_2 in air with 95% humidity.

At 70% confluence (passage range 8-15) H9c2 cells were harvested and cell viability was determined by trypan blue exclusion. Cell concentration was determined by means of a Neubauer haemocytometer (depth: 0.1 mm, area: 0.04 mm^2).

D. Temperature monitoring during applied ultrasound

Temperature was measured on the external surface of the PZT transducer by means of a digital thermometer, while the microdevice was filled with cell culture medium. Recordings were taken over the range of 0-40 V peak-to-peak (V_{pp}) and at 1 min time intervals. Both temperature trend and maximum temperature variation were quantified.

E. Cell viability in the absence (CA-free) and presence of ultrasound contrast agent

Harvested H9c2 cells in serum-free medium were placed in a 1 ml syringe at a concentration of 2×10^6 cells/ml. Cell viability was established under both static conditions (i.e., cells seeded directly onto a sterile microtitre well plate) and continuous-flow (inlet flow rate, $Q_{in} = 0.1$ ml/min) at 0, 10, 20, 30, and 40 peak-to-peak voltage (V_{pp}), in both the presence and absence (CA-free) of contrast agent. For each amplitude, 1 ml of cell suspension was collected in individual sterile flasks and dispensed (100 μl $\times$ 6 repeats) with a multichannel pipette into corresponding rows of the microtitre well plate and incubated at 37 °C. Cell viability was determined by propidium iodide (PI) assay. PI (10 μM) was added to the cell suspension and the fluorescence intensity ($\lambda_{exc} = 485$ nm, $\lambda_{em} = 510$ nm) was quantified using a FLUOstar Omega plate reader, and data processed using Omega v. 1.20 and Mars data analysis v. 2.00. For establishing cell viability in the presence of CA, an average concentration of 33 bubbles/cell was added to the cell suspension.[36] Additionally, acoustic pressure levels employed in the present study fall into the range of acoustic pressure to which CAs are exposed *in vivo*.[37]

F. Single-cell analysis of CA-free cell sonoporation

Single-cell analysis was performed in order to investigate CA-free cell sonoporation using CMFDA, an intracellular low-molecular size (464.86 MW) membrane-impermeable fluorescent probe. The reduction of intracellular fluorescence intensity was quantified as an indicator of *in situ* CMFDA efflux induced by cell sonoporation.

1. Minimisation of CMFDA photobleaching

In order to determine CMFDA efflux induced by CA-free sonoporation, quantification of superfluous intracellular CMFDA photobleaching was required.

Prior to harvesting, H9c2 cells were incubated with 5 μM CMFDA (in fresh serum free medium) at 37 °C. After 45 min, the medium containing CMFDA was aspirated and replaced

with fresh medium, and cells were incubated for a further 30 min to allow cell recovery. Cells were then harvested and placed in a 5 ml plastic syringe and infused into the device. Cells were imaged in the absence of ultrasound but exposed to fluorescent light ($\lambda_{exc} = 485$ nm). A pulsed fluorescent light ($\Delta t = 1$ min, synchronized with the CCD camera) at varying exposure times ($t_{exp} = 150$, 200, and 300 ms) was applied in order to quantify the photobleaching. The fluorescence emitted by intracellular CMFDA was measured by sampling a minimum of 10 individual cells at each exposure time. Intracellular fluorescence intensity was quantified using an automated *in house* MATLAB-based code (The MathWorks Inc., MA).

2. CMFDA efflux by CA-free cell sonoporation

CMFDA loaded cells were injected within the microfluidic device and allowed time to migrate towards the nodal plane [Fig. 1(c)] prior to imaging. Migration was estimated to be 1-3 s, depending on the excitation voltage. Fluorescent images of single cells were captured at 1 min time intervals, at varying excitation voltages (3.2, 5.6, and 9.2 V_{pp}). Images at each voltage were obtained on different days in order to eliminate intracellular CMFDA degradation over the experimental duration, and voltages were not selected incrementally. After correcting for photobleaching, intracellular fluorescence intensity was quantified using an *in house* MATLAB-based code.

G. Retrospective analysis

1. Drug cytotoxicity comparison pre- and post-sonications

The intracellular delivery of low- (apigenin 270.24 and luteolin 286.24) and intermediate- (doxorubicin 543.52) molecular weight therapeutic agents, induced by CA-free cell sonoporation, was investigated through *retrospective* post-sonication analysis. Therapeutic agents include doxorubicin which has known cardiotoxic activity,[38] apigenin which has known cardioprotective activity[39] and luteolin which is a known active metabolite of apigenin.[40] The drug concentration (100 μM) was established from a short incubation (4 h, minimum time to allow for cell adhesion) cytotoxicity curve (data not shown) for apigenin (the least active of the three compounds) in order to identify a concentration that would elicit marginal cell toxicity (IC_{25}) pre-sonication. This concentration was then applied with luteolin and doxorubicin in order to observe whether CA-free sonoporation was achievable for structurally diverse drug molecules, regardless of their initial or intrinsic toxicity.

Harvested H9c2 cells were suspended at a density of 2×10^6 cells/ml and were placed on ice until just prior to the addition of either doxorubicin, apigenin, or luteolin. Aliquots (1 ml) of the suspended cells were placed in separate 1 ml syringes immediately upon the addition of each drug, followed by infusion ($Q_{in} = 0.1$ ml/min) into the US device. Following infusion, samples (exposed to either, 0, 10, 20, 30, or 40 V_{pp}) were recaptured in sterile containers and dispensed into a microtitre well plate. Controls consisted of either cells seeded directly into the microtitre well plate, cells infused into the device in the absence of drug, or cells infused into the device in the absence of both drug and US. All cells were subsequently incubated for 4 h to allow cell adhesion, followed by a further 1.5 h incubation in the presence of MTT (50 μl of 1 mg/ml solution). All medium was then aspirated and the resulting MTT formazan product was solubilised in 150 μM of DMSO. MTT absorbance ($\lambda_{abs} = 540$ nm) was quantified using a FLUOstar Omega plate reader, and data processed using Omega v. 1.20 and Mars data analysis v. 2.00.

2. CA-free ultrasound-induced FITC-dextran uptake

The intracellular delivery of high-molecular weight FITC-dextran fluorescent probe (40 kDa), induced by CA-free cell sonoporation, was investigated through *retrospective* post-sonication analyses.

Harvested H9c2 cells were placed in 1 ml syringes containing 0.5 ml cell serum-free medium and 0.5 ml of 0.25 mg/ml (final concentration) FITC-dextran, in sterile phosphate buffer

and with a cell concentration of 2×10^6 cells/ml. Control cells were incubated at room temperature with FITC-dextran, in the absence of ultrasound. Experimental cells were infused into the device at $Q_{in} = 0.1$ ml/min. Intracellular FITC-dextran was quantified by measuring sample absorbance at $\lambda_{abs} = 490$ nm, using a FLUOstar Omega plate reader. Data were processed using Omega v. 1.20 and Mars data analysis v. 2.00.

III. RESULTS AND DISCUSSION

A. Microfluidic device characterisation

An USW was generated within the microfluidic device. Electrical impedance measurements showed a minimum in the impedance spectrum at the resonant frequency (f_R) of 2.27 MHz (data not shown), which was subsequently selected as the working frequency. Impedance measurements were repeated prior to each experiment to ensure consistent operating conditions, and only slight variations in resonant frequency ($\Delta f_R = \pm 0.03$ MHz) were observed over the course of the experiments described here.

The acoustic pressure (P) within the capillary, measured through drop-voltage analysis, was calculated to be $3.47 \times 10^4 \times V_{pp}$ Pa, with the excitation voltage, V_{pp}, varying between 3.2 and 40 V_{pp}. This corresponded to pressures in the range of 0.11–1.39 MPa.

The US environmental temperature was monitored to ensure that biologically compatible temperatures were maintained. Figure SI1(a) in the supplementary information[41] shows temperature recordings over 0–15 min. At 10 V_{pp} the temperature increased gradually from ambient, varying between 21 and 23 °C, up to 25 °C over the first 6 min then plateaued. Long-term ($t_{end} = 4$ h), this plateau was maintained until recording ceased. However, at 30 V_{pp} the temperature increased more steeply from ambient, reaching a plateau at ~38 °C [inset, Fig. SI1(a) in the supplementary information[41]]. Therefore, it is reasonable to assume that thermal mechanisms do not contribute to either cell sonoporation or reduced cell viability at the lower V_{pp} employed in the present study. However, the contribution of thermal mechanisms[42] on membrane poration or cell viability cannot be completely excluded at the higher voltages.

Whilst US-induced increase of the local temperature has been already reported as a potential facilitating agent of cell membrane permeabilization,[43,44] the contribution of temperature elevation on the formation of transmembrane pores remains unclear.[45]

B. Cell viability in the absence (CA-free) and presence of ultrasound contrast agent

A comparison of cell viability in both the absence and presence of CA (Fig. 2) revealed that at lower amplitudes ($V_{pp} \leq 20$) no significant difference in viability between CA-free and CA-based US exposure was observed. However, at higher amplitudes ($V_{pp} > 20$) viability was significantly reduced in the presence of CA, in agreement with Chen *et al.*[46] This is maybe due to the increased cavitation activity associated with CAs.[46,47] Cell viability following US-induced membrane poration in the absence of CA remains largely overlooked and as such, cell viability is generally reported in terms of the combined effect of US with CA rather than the effects of US "alone."[48] Additionally, commercially available CAs appear to have varying threshold levels before inducing cell death.[49] Cell death mechanisms (apoptosis, necrosis, autolysis, autophagy, and oncosis) display considerable overlap,[50] adding further complexity. Therefore, further research is required in order to delineate the concomitant contribution of CA and US on cell viability and the way in which they bring about cell death.

C. Single-cell analysis: Real-time intracellular CMFDA efflux induced by CA-free cell sonoporation

1. Minimisation of CMFDA photobleaching

In order to quantify sonoporation by efflux measurements of the fluorescent probe CMFDA from the intracellular to the extracellular environment, the fluorescence photobleaching of CMFDA was firstly quantified.[41] At three different fluorescent exposure times ($t_{exp} = 150$, 200,

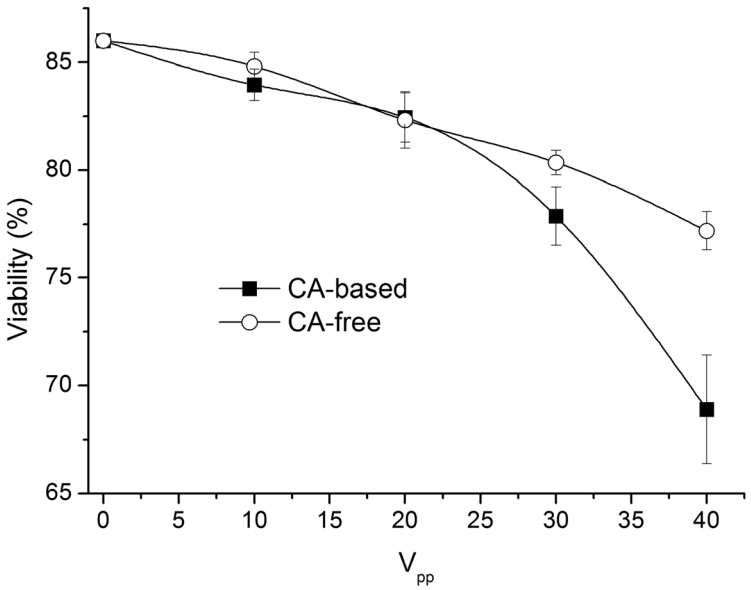

FIG. 2. H9c2 cell % viability measured in the absence (blank circle) and in the presence (filled square) of CA. Data at 0, 10, 20, 30, and 40 V_{pp} are reported (n = 6 at each V_{pp}). At $V_{pp} \leq 20$ CA-free and CA-based cell viability display similar values. At $V_{pp} > 20$ CA-free and CA-based cell viability diverge, with CA-free US exposure maintaining higher viability, compared with CA-based US exposure.

and 300 ms) photobleaching showed a linear-like trend (data not shown). Experimental data were averaged and linearly interpolated ($R^2 > 0.95$ in all cases). The absolute value of the interpolation slope (defined as a bleaching coefficient, β) was observed to linearly vary with t_{exp}, with higher exposure times producing enhanced bleaching [Fig. SI1(b) in the supplementary information[41]]. Additionally, β showed that the rate of CMFDA photobleaching was slower than the rate of CMFDA efflux by sonoporation, thus quantitative sonoporation was possible.

2. CMFDA efflux by CA-free sonoporation

The dynamics of CA-free single-cell sonoporation was evaluated by measuring the real-time reduction of intracellular fluorescent CMFDA at 3.2, 5.6, and 9.2 V_{pp}. However, despite consistent US operating conditions, this reduction in fluorescence consistently showed two reproducible temporal trends [Fig. 3(a)] throughout the range of V_{pp} investigated. The trends were assigned as exponential-like (Group A) and parabolic-like (Group B) [Fig. 3(a)]. The average interpolation functions were determined as follows (R^2 was > 0.9 in all cases examined):

$$FI_{norm}(t) = e^{-K_A t} \qquad (\text{Group A}), \tag{1}$$

$$FI_{norm}(t) = K_B t^2 + C_1 t + 1 \qquad (\text{Group B}), \tag{2}$$

where FI_{norm} is the intracellular fluorescence intensity normalised to the initial value, $FI(0)$; t is the time (minutes); C_1 is a numeric constant; K_A and K_B are parameters assumed here as indicators of sonoporation dynamics (i.e., CMFDA efflux) for cells located in Group A and Group B, respectively. K_A was observed to increase significantly by increasing the applied V_{pp} from 3.2 to 5.6 ($K_A = 0.164\,\text{min}^{-1}$ and $0.212\,\text{min}^{-1}$ at $V_{pp} = 3.2$ and 5.6, respectively); however, only a marginal increase was detected by further increasing the V_{pp} ($K_A = 0.212\,\text{min}^{-1}$ and $0.231\,\text{min}^{-1}$ at $V_{pp} = 5.6$ and 9.2, respectively) [Fig. 4(b)]. K_B instead showed a significant increase only at $V_{pp} = 9.2$ (in respect to lower amplitudes) [Fig. 4(b), blank circle].

The reason for the emergence of these two trends is unknown; however, a theoretical model proposed by Krasovitski *et al.* may explain the experimental observations.[51] The

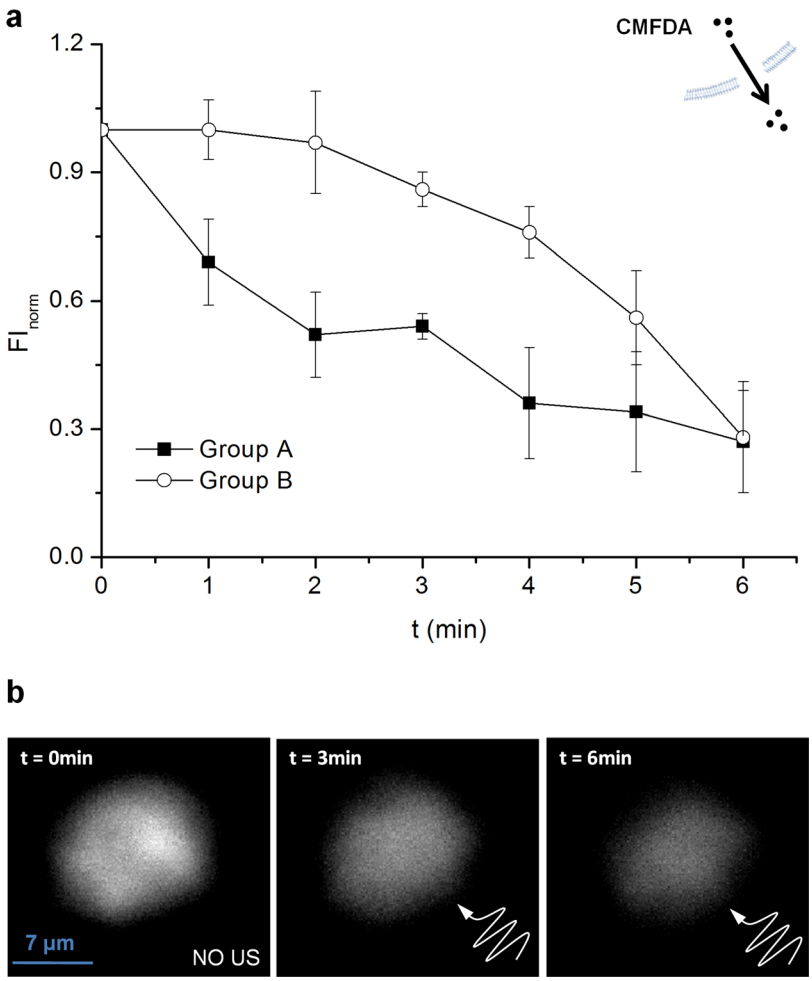

FIG. 3. Fluorescent microscopy-based analysis of CMFDA efflux from H9c2 cells. (a) Intracellular normalized fluorescence intensity of CMFDA at time intervals of 1 min (USW exposure = 6 min). CA-free sonoporation induces the transfer of CMFDA from the intracellular to the extracellular milieu (inset). Reduction in intracellular fluorescence shows a biphasic cell response. The two characteristic trends are reported: Group A (exponential-like, filled square) and Group B (parabolic-like, blank circle), at 9.2 V_{pp} (n = 10 at each V_{pp}). (b) Representative microscope fluorescent images (50 × magnification) at 0, 3, and 6 min (V_{pp} = 9.2).

exponential-like decay may correspond to an immediate short-term response of the cell membrane upon initial US exposure, potentially leading to sudden membrane permeabilization. Krasovitski's model suggests that large membrane strain thresholds are reached immediately after US exposure commences (at 0.2 and 0.8 MPa acoustic pressures), due to a vibrational mechanism described as intramembranous cavitation.[51] Notably, the acoustic pressure exerted on the cell membrane within our microdevice (in the range of 0.11-1.39 MPa) whilst travelling towards the nodal plane,[52] may be among the potential mechanisms leading to the observed short-term membrane poration resulting in the exponential-like efflux of CMFDA.

Our findings show that short-term CA-free membrane sonoporation occurs at relatively low V_{pp} [Fig. 4(a)] and that by increasing V_{pp} results in a non-linear increase of short-term sonoporation rate [Fig. 4(b), filled circle]. In this respect, we can hypothesise that over a critical V_{pp} CA-free short-term sonoporation dynamics remains substantially unvaried, and CMFDA efflux is regulated by passive diffusion through transmembrane pores.

Conversely, an explanation for long-term membrane response has not been put forward so far. However, we hypothesize that the parabolic-like CMFDA efflux may be the result of such long-term membrane response to US. This hypothetical long-term response may be induced by

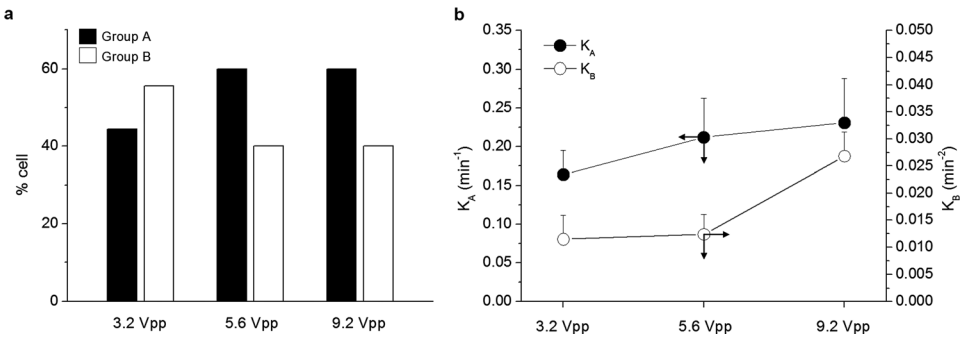

FIG. 4. Real time, single cell analysis of the dynamics of US-induced CMFDA efflux by H9c2 cells, in the absence of CA. CMFDA transfer from the intracellular to the extracellular milieu showed two distinct reproducible trends. (a) Percentage of cells in Group A and Group B, at three different V_{pp}. CA-free sonoporation dynamics is quantified by calculating K_A (min^{-1}) and K_B (min^{-2}) values, at different V_{pp} (b); n = 10 at each V_{pp}. Both K_A and K_B increased with increasing V_{pp}.

a fatigue condition generated by the periodic expansions and contractions of the membrane leaflets, which is in agreement with Krasovitski's intramembranous cavitation concept. This cyclic intramembranous strain condition may be responsible for the formation of transmembrane pores that occurs only after the cell membrane is subjected to a critical number of strain cycles.

Experimental observations suggest that the dynamics of long-term CA-free sonoporation varied significantly only at V_{pp} higher than a critical value (i.e., $V_{pp} > 5.6$ in our microdevice) [Fig. 4(b)], thus implying the existence of interplay between the number of strain cycles and the absolute value of membrane strain (which will depend on the applied V_{pp}). In addition, the onset of non-inertial streaming[53] at the nodal plane (experimentally observed at $V_{pp} > 7$) may contribute to additional fluid shear stress on the cell membrane, thus enhancing or facilitating long-term membrane response described above. Until further research is undertaken, the observed bi-phasic dynamics of membrane CA-free sonoporation can only be explained theoretically. Krasovitski's intramembranous cavitation model provides a good conceptual correlation with our experimental observations, but further experimental assessment is required.

3. Average CMFDA efflux dynamics

The average reduction of intracellular CMFDA fluorescence intensity (ΔFI_{norm}) with respect to the applied V_{pp} was measured at 2, 4, and 6 min from the onset of US exposure (Fig. 5). The results show that, at 3.2 V_{pp}, longer US exposure times ($t \geq 2$ min) were required to initiate a measurable reduction of CMFDA by CA-free cell sonoporation ($\Delta FI_{norm} = 0.27$ after 6 min). In contrast, at 5.6 and 9.2 V_{pp}, a more significant reduction of intracellular CMFDA was observed, and over shorter US exposure times ($\Delta FI_{norm} = 0.35$ and 0.41, respectively, after 4 min). Additionally, ΔFI_{norm} was observed to saturate with increasing V_{pp} (a non-linear relationship occurred between ΔFI_{norm} and V_{pp}) (Fig. 5).

A representative average trend of the intracellular CMFDA fluorescence intensity (FI_{norm}), at $V_{pp} = 5.6$, is shown in the inset of Figure 5. Fluorescence data are plotted together with the corresponding standard deviation and control trend (established from photobleaching measurements). An analytical formulation was established in order to describe the average FI_{norm}-t relationship

$$FI_{norm} \cong 1 \qquad \text{for } t \leq t_0, \tag{3}$$

$$FI_{norm} = -K_T \cdot t + C_2 \qquad \text{for } t \geq t_0, \tag{4}$$

where t_0 is equal to 0, 1, and 2 min for V_{pp} of 9.2, 5.6, and 3.2, respectively; C_2 is a numeric constant; K_T is equal to 0.12, 0.11, and 0.08 min^{-1} for V_{pp} of 9.2, 5.6, and 3.2 respectively, and represents a quantitative estimation of the average CMFDA efflux dynamics, depending on the

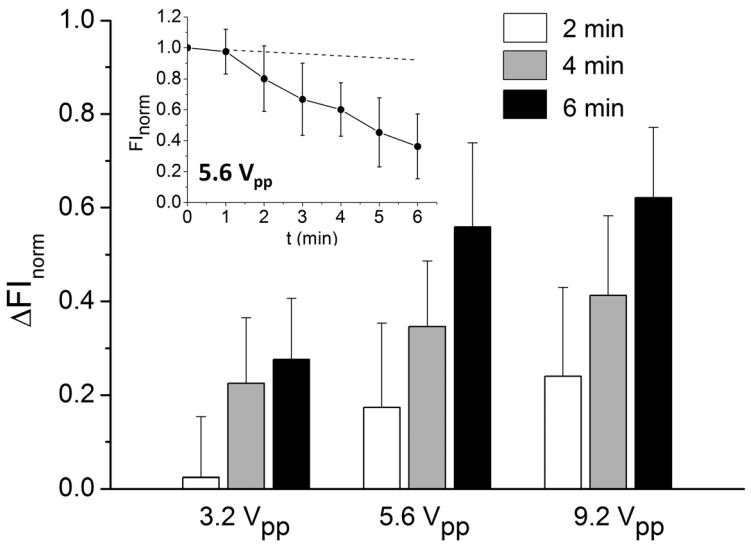

FIG. 5. Evaluation of CMFDA efflux by single-cell analysis. The average reduction of intracellular fluorescent intensity (ΔFI_{norm}) at 3.2, 5.6, and 9.2 V_{pp} is shown. ΔFI_{norm} values at 2, 4, and 6 min from the onset of the USW are reported. A representative intracellular fluorescence (FI_{norm}) decay is also shown (inset), corresponding to $V_{pp} = 5.6$. n = 10 at each V_{pp}.

mutual contribution of CA-free short-term sonoporation and CA-free long-term sonoporation → $K_T = K_T(K_A, K_B)$.

The results show that intracellular CMFDA fluorescence remained approximately constant (~ 1) until a critical time instant (t_0), and decreased following a linear-like function ($R^2 > 0.95$) for $t > t_0$; where $t_0 = t_0(V_{pp})$. The average CMFDA efflux rate was observed to increase non-linearly with the applied voltage. These observations are supported by the V_{pp}-dependence of both long-term and short-term sonoporation dynamics, illustrated in Figure 4(b), with higher voltages favouring short-term mechanisms [Fig. 4(a)].

These results suggest that higher V_{pp} provide efficient ultrasonically induced efflux of CMFDA (Fig. 5). However, the efficiency of CMFDA efflux (ΔFI) is subjected to saturation (and likely the mass transfer of similar molecules) and any further increase of V_{pp} over the saturation limit risks compromising cell viability.

Notably, the efficiency of mass transfer will also vary according to the device design and physical ultrasonic parameters (i.e., working frequency), which require characterization for a given device configuration.

D. Retrospective analysis

1. Drug cytotoxicity comparison pre- and post-sonications

The CA-free ultrasound induced uptake of doxorubicin, apigenin, and luteolin was observed to be facilitated by measuring their respective cytotoxic action pre- and post-sonications.

Retrospective analysis of cell cytotoxicity (measured by traditional MTT assay) in the presence of doxorubicin both pre- and post-sonications [Fig. 6(a)] showed that doxorubicin cytotoxicity increased by 25%, 55%, 91%, and 85% post-sonication at 10, 20, 30, and 40 V_{pp}, respectively, in respect to doxorubicin in the absence of US. In the presence of apigenin, cytotoxicity increased by 2%, 24%, 40%, and 50% post-sonication at 10, 20, 30, and 40 V_{pp}, respectively, in respect to apigenin in the absence of US [Fig. 6(b)]. The cytotoxicity of luteolin, an active metabolite of apigenin, increased by 15%, 83%, 89%, and 90% post-sonication at 10, 20, 30, and 40 V_{pp}, respectively, in respect to luteolin in the absence of US [Fig. 6(c)].

Cytotoxicity-V_{pp} relationship was investigated by introducing a coefficient (cytotoxic coefficient, *Cyt*) defined as: 1-[$cs(V_{pp})/cs(control)$], where $cs(V_{pp})$ corresponds to cell survival (in %) measured at a given V_{pp}, and $cs(control)$ corresponds to cell survival (in %) measured at 0 V_{pp}

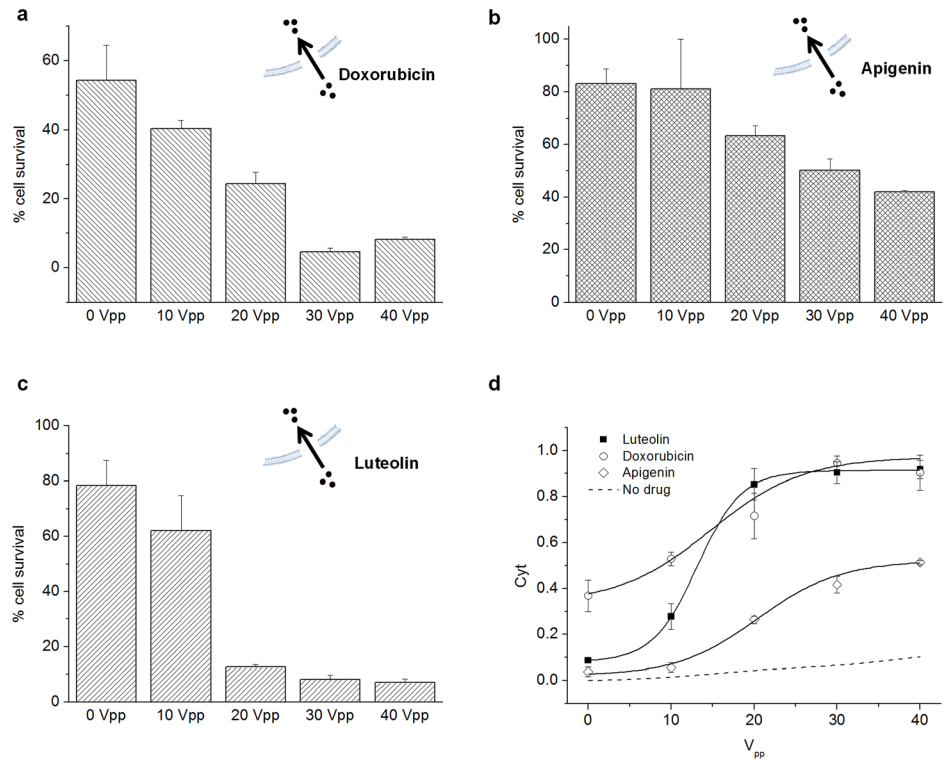

FIG. 6. The facilitated uptake of pharmaceutical agents, from the extracellular to the intracellular environment, was quantified through cytotoxicity measurement. Percentage of cell survival was quantified as an indicator of cell uptake of doxorubicin (a), luteolin (b), and apigenin (c); at 0, 10, 20, 30, and 40 V_{pp}. Controls corresponded to 0 V_{pp} and no extracellular drug; n = 6 at each V_{pp}. (d) *Cyt*-V_{pp} relationship was plotted for each drug, showing that, although each drug displays different initial (no US) cytotoxicity, the toxicity in all cases increased with increasing V_{pp}. Control cells in the absence of drug are shown by dotted line.

in the absence of both US and drugs. Figure 6(d) shows the experimental *Cyt* values at different V_{pp} together with the interpolation curve (spline interpolation). The results show that CA-free sonoporation induced an increase in the cytotoxic action of doxorubicin, apigenin, and luteolin suggesting that the uptake was facilitated with respect to toxicity occurring through passive diffusion [Figs. 6(a)–6(c)]. *Cyt* showed a non-linear dependence on the applied voltage where cytotoxic action increased with increasing V_{pp} until a plateau level was reached, which is in agreement with our s*ingle-cell* analyses. The observed plateau could be attributed to either mass transfer saturation (as observed in *single-cell* experiments) or a biological effect such as enzyme inhibition due to active site saturation.

These results indicate that by increasing V_{pp} above 30 V does not further facilitate drug uptake and may also potentially compromise cell viability.

2. CA-free ultrasound-induced FITC-dextran uptake

The delivery of a high-molecular weight fluorescent probe (FITC-dextran, 40 kDa) induced by CA-free sonoporation was investigated. Figure 7 shows the percentage of intracellular FITC-dextran at different 0, 10, 20, 30, and 40 V_{pp}. In order to quantify intracellular FITC-dextran only, absorbance of the extracellular FITC-dextran (in medium) was quantified and subtracted from the total absorbance of the sample. Controls in static conditions and continuous-flow were undertaken in order to assess the contribution of spontaneous diffusion and of flow shear stress on FITC-dextran mass transfer, respectively (inset, Fig. 7). The results show that marginal diffusion occurred due to the effect of flow shear stress on the cell membrane (inset, Fig. 7).

An increase in intracellular FITC-dextran with increasing V_{pp} was also observed (Fig. 7). However, a significant increase was only evident at $V_{pp} > 20$, further corroborating the observed

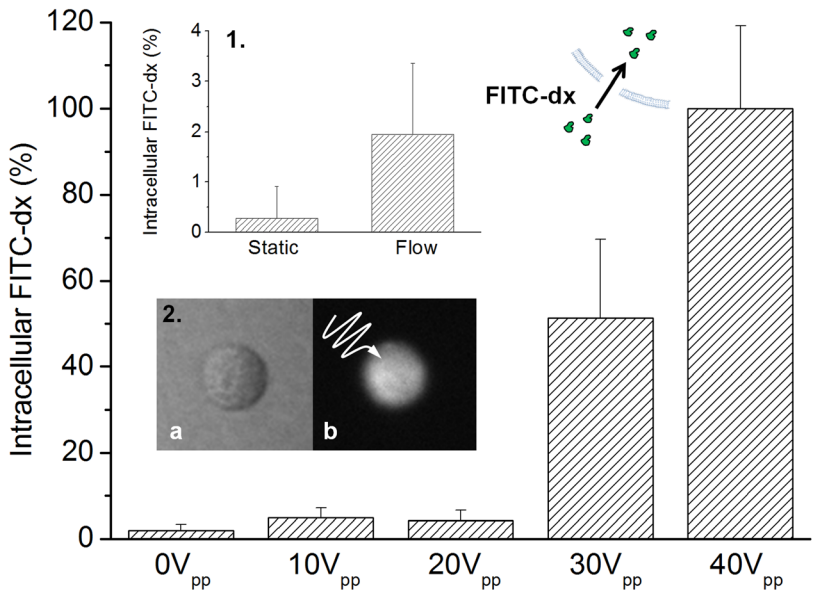

FIG. 7. Transmembrane transfer of FITC-dextran (40 kDa) induced by CA-free sonoporation. Intracellular FITC-dextran % at 0, 10, 20, 30, and 40 V_{pp} is shown. The comparison between static condition and continuous-flow condition (no US) (inset 1) shows that the contribution of fluid-shear stress on transmembrane transfer of FITC-dextran was observed and was negligible. Representative microscope images (20 ×magnification) of a single suspended H9c2 cardiomyoblast (inset 2(a), bright field image; 2(b), fluorescent image) are shown after CA-free sonoporation at 30 V_{pp}; n = 4 at each V_{pp}.

non-linear dependence of mass transfer efficiency on the applied V_{pp}. Furthermore, the results show that high-molecular weight FITC-dextran required higher V_{pp} to be delivered intracellularly by CA-free sonoporation, compared to the relatively smaller agents, apigenin, luteolin, or doxorubicin, suggesting a complex interrelationship between the efficiency of mass transfer, pore size, and the applied V_{pp}. CA-free sonoporation within our microfluidic device allowed the transmembrane transfer of high-molecular weight molecules, having comparable size with bioactive macromolecules such as DNA fragments, siRNA, and proteins.

IV. CONCLUSIONS

CA-free cell sonoporation was investigated by generating an USW within a microfluidic device. Both real time *single-cell* analysis and *retrospective* post-sonication analysis revealed successful transmembrane transport of differently sized molecules, without the need for expensive contrast agents and thus avoiding the associated cavitational effects which significantly compromise cell viability. This microfluidic-based strategy allowed fine control of the fluidic environment (i.e., low Reynolds number), whilst the USW allowed precise regulation of the US stimulus and *in situ* microscope-based monitoring of individual cells located at the nodal plane. In addition, the continuous-flow condition allowed for the processing of relatively large numbers of cells without exerting significant additional stress on the cell membrane.

Crucially, by combining these strategies, we were able to demonstrate, for the first time, the facilitated up-take of potentially beneficial pharmaceutical agents by cytotoxic measurements both pre- and post- sonications. In the current economic climate this low-cost US-microfluidic device provides an alternative to other more expensive techniques for transmembrane drug delivery, such as laser irradiation.[35] Additionally, our strategy provides an *in vitro* alternative to controversial *in vivo* models used for early stage drug discovery, drug delivery programs, and toxicity measurements.

Interestingly, single-cell analyses within our microfluidic device have suggested the existence of different biophysical mechanisms contributing to US-induced membrane response in the absence of CA. In this regard, further studies are currently under investigation in our

laboratories in order to gain a deeper understanding of the mechanisms regulating CA-free cell sonoporation; an area that has been largely overlooked since most sonoporation studies include CA. As such it has been difficult to precisely delineate US effects from CA effects on cell viability and membrane stress response. We will also be investigating ways of coupling our US microfluidic-based device with high throughput screening systems and high-resolution bio-analytical methodologies.

ACKNOWLEDGMENTS

We would like to thank the Engineering and Physical Sciences Research Council (EPSRC) for funding this research (Grant reference No. EP/H01392X/1).

[1]K. Kooiman, M. Foppen-Harteveld, A. F. W. der Steen, and N. de Jong, J. Controlled Release **15**(1), 35 (2011).
[2]W. L. Nyborg, Ultrasound Med. Biol. **32**(10), 1557 (2006).
[3]J. H. Hwang, A. A. Brayman, M. A. Reidy, T. J. Matula, M. B. Kimmey, and L. A. Crum, Ultrasound Med. Biol. **31**(4), 553 (2005).
[4]J. Wu and W. L. M. Nyborg, *Emerging Therapeutic Ultrasound* (World Scientific Pub Co. Inc., Singapore, 2006).
[5]J. Wu, J. Pepe, and M. Rincón, Ultrasonics **44**, e21 (2006).
[6]C. D. Ohl, M. Arora, R. Ikink, N. De Jong, M. Versluis, M. Delius, and D. Lohse, Biophys. J. **91**(11), 4285 (2006).
[7]H. Y. Wang and C. Lu, Anal. Chem. **78**(14), 5158 (2006).
[8]A. Noori, P. R. Selvaganapathy, and J. Wilson, Lab Chip **9**(22), 3202 (2009).
[9]A. Uchugonova, K. König, R. Bueckle, A. Isemann, and G. Tempea, Opt. Express **16**(13), 9357 (2008).
[10]Y. W. Han, A. Ikegami, P. Chung, L. Zhang, and C. X. Deng, Appl. Environ. Microbiol. **73**(11), 3677 (2007).
[11]N. Bose, D. Carugo, T. K. Maiti, X. Zhang, and S. Chakraborty, Presented at the MicroTAS 2011, Seattle (in press).
[12]D. Dalecki, Annu. Rev. Biomed. Eng. **6**, 229 (2004).
[13]G. J. Liu, M. D. Lu, X. Y. Xie, H. X. Xu, Z. F. Xu, Y. L. Zheng, J. Y. Liang, and W. Wang, J. Ultrasound Med. **27**(4), 657 (2008).
[14]M. Postema, A. Van Wamel, C. T. Lancée, and N. De Jong, Ultrasound Med. Biol. **30**(6), 827 (2004).
[15]A. A. Brayman, M. Azadniv, C. Cox, and M. W. Miller, Ultrasound Med. Biol. **22**(7), 927 (1996).
[16]C. R. Mayer and R. Bekeredjian, Adv. Drug Delivery Rev. **60**(10), 1177 (2008).
[17]R. Bekeredjian, P. A. Grayburn, and R. V. Shohet, J. Am. Coll. Cardiol. **45**(3), 329 (2005).
[18]S. Armstrong and C. E. Ganote, Cardiovasc. Res. **28**(7), 1049 (1994).
[19]B. Kimes and B. Brandt, Exp. Cell Res. **98**(2), 367 (1976).
[20]B. N. M. Zordoky and A. O. S. El-Kadi, J. Pharmacol. Toxicol. Methods **56**(3), 317 (2007).
[21]W. M. S. Russell and R. L. Burch, Methuen & Co. Ltd., London (1959).
[22]S. Creton, I. C. Dewhurst, L. K. Earl, S. C. Gehen, R. L. Guest, J. A. Hotchkiss, I. Indans, M. R. Woolhiser, and R. Billington, Crit. Rev. Toxicol. **40**(1), 50 (2010).
[23]S. Khanna, N. N. Amso, S. J. Paynter, and W. T. Coakley, Ultrasound Med. Biol. **29**(10), 1463 (2003).
[24]Y. Lee and C. Peng, Gene Ther. **12**(7), 625 (2005).
[25]S. Rodamporn, N. R. Harris, R. Boltryk, S. P. Beeby, and T. Sanchez-Elsner, IEEE Trans. Biomed. Eng. **58**(4), 927 (2010).
[26]M. Kinoshita and K. Hynynen, Biochem. Biophys. Res. Commun. **359**(4), 860 (2007).
[27]M. A. Hassan, M. A. Buldakov, R. Ogawa, Q. L. Zhao, Y. Furusawa, N. Kudo, T. Kondo, and P. Riesz, J. Controlled Release **141**(1), 70 (2010).
[28]D. Carugo, D. N. Ankrett, L. Capretto, P. Glynne-Jones, R. Boltryk, P. Townsend, X. Zhang, and M. Hill, Presented at the MicroTAS 2011, Seattle (in press).
[29]S. Mazzitelli, L. Capretto, D. Carugo, X. Zhang, R. Piva, and C. Nastruzzi, Lab Chip **11**(10), 1776 (2011).
[30]L. Capretto, D. Carugo, W. Cheng, M. Hill, and X. Zhang, J. Colloid Interface Sci. **357**(1), 243 (2011).
[31]X. Zhang, H. Yin, J. M. Cooper, and S. J. Haswell, Electrophoresis **27**(24), 5093 (2006).
[32]P. Mary, L. Dauphinot, N. Bois, M. C. Potier, V. Studer, and P. Tabeling, Biomicrofluidics **5**, 024109 (2011).
[33]B. Hammarström, M. Evander, H. Barbeau, M. Bruzelius, J. Larsson, T. Laurell, and J. Nilsson, Lab Chip **10**(17), 2251 (2010).
[34]P. Glynne-Jones, R. J. Boltryk, M. Hill, F. Zhang, L. Dong, J. S. Wilkinson, T. Melvin, N. R. Harris, and T. Brown, Anal. Sci. **25**(2), 285 (2009).
[35]S. Mehier-Humbert and R. H. Guy, Adv. Drug Delivery Rev. **57**(5), 733 (2005).
[36]M. Ward, J. Wu, and J. F. Chiu, Ultrasound Med. Biol. **26**(7), 1169 (2000).
[37]M. A. Hassan, P. Campbell, and T. Kondo, Drug Discovery Today **15**(21–22), 892 (2010).
[38]B. N. M. Zordoky and A. O. S. El-Kadi, Vascular Pharmacol. **49**(4–6), 166 (2008).
[39]B. Jin, L. Qian, S. Chen, J. Li, H. Wang, I. C. Bruce, J. Lin, and Q. Xia, Eur. J. Pharmacol. **616**(1–3), 200 (2009).
[40]V. P. Androutsopoulos, K. Ruparelia, R. R. J. Arroo, A. M. Tsatsakis, and D. A. Spandidos, Toxicology **264**(3), 162 (2009).
[41]See supplementary material at http://dx.doi.org/10.1063/1.3660352 for temperature recordings and CMFDA bleaching coefficient values.
[42]K. G. Baker, V. J. Robertson, and F. A. Duck, Phys. Ther. **81**(7), 1351 (2001).
[43]H. D. Liang, Q. L. Lu, S. A. Xue, M. Halliwell, T. Kodama, D. O. Cosgrove, H. J. Stauss, T. A. Partridge, and M. J. K. Blomley, Ultrasound Med. Biol. **30**(11), 1523 (2004).
[44]C. C. Coussios, C. Farny, G. Ter Haar, and R. Roy, Int. J. Hyperthermia **23**(2), 105 (2007).
[45]V. G. Zarnitsyn and M. R. Prausnitz, Ultrasound Med. Biol. **30**(4), 527 (2004).

[46]W. S. Chen, A. A. Brayman, T. J. Matula, and L. A. Crum, Ultrasound Med. Biol. **29**(5), 725 (2003).
[47]Y. Qiu, Y. Luo, Y. Zhang, W. Cui, D. Zhang, J. Wu, J. Zhang, and J. Tu, J. Controlled Release **145**(1), 40 (2010).
[48]L. B. Feril, Ultrasound Med. Biol. **29**(2), 331 (2003).
[49]D. L. Miller and J. Quddus, Ultrasound Med. Biol. **26**(4), 661 (2000).
[50]T. M. Scarabelli, R. Knight, A. Stephanou, P. Townsend, C. Chen-Scarabelli, K. Lawrence, R. Gottlieb, D. Latchman, and J. Narula, Curr. Probl. Cardiol. **31**(3), 181 (2006).
[51]B. Krasovitski, V. Frenkel, S. Shoham, and E. Kimmel, Proc. Natl. Acad. Sci. U.S.A. **108**(8), 3258 (2011).
[52]R. Townsend, M. Hill, N. Harris, and N. White, Ultrasonics **42** (1–9), 319 (2004).
[53]L. A. Kuznetsova and W. T. Coakley, J. Acoust. Soc. Am. **116**, 1956 (2004).